Layered Ta_2NiS_5 Q-Switcher for Mid-Infrared Fluoride Fiber Laser

Qinwen Duan, Lingling Yang, Yuan He, Longlong Chen, Jie Li, Lili Miao [ID], and Chujun Zhao [ID]

Abstract—We have demonstrated the stable Q-switched Er-doped fluoride fiber laser with the help of the few-layered Ta_2NiS_5 in the mid-infrared spectral range. We fabricated the mid-infrared saturable absorber mirror (SAM) by depositing the layered Ta_2NiS_5 on a gold mirror. The layered Ta_2NiS_5 exhibited saturable absorption behavior with modulation depth 36% and saturation intensity 32.2 GW/cm^2 at 2800 nm, respectively. With the Ta_2NiS_5-SAM, stable Q-switched pulses around 2.8 μs wavelength can be delivered with a pulse duration of 1.20 μs and a repetition rate of 102 kHz under an incident pump power of 860 mW from the ZBLAN fiber laser cavity. The experimental results confirm that Ta_2NiS_5 has great potentials as broadband saturable absorber in mid-infrared regions, paving the way for the application of low-dimensional ternary chalcogenide in broadband optoelectronic devices.

Index Terms—Infrared lasers, fiber lasers, Q-switched lasers, optoelectronic materials.

I. INTRODUCTION

THE pulsed mid-infrared (MIR) fiber laser sources can cover the absorption window of the molecular fingerprints of the gases, liquids and solids [1], [2], which are highly required for the versatile applications ranging from laser microsurgery, remote atmosphere sensing, environmental detection to laser radar, etc. With the evolution of the high-power MIR fiber laser, the Er^{3+}-doped ZBLAN fiber laser has aroused extensive attentions for the high slope efficiency due to the effective energy-transfer up-conversion process. By integrating the nonlinear absorption characteristics of the saturable absorber (SA) into the laser cavity, the Er-doped fluoride fiber laser can be modulated to deliver the optical pulses. However, the immature nonlinear optical modulators hinder the performance improvement of the pulsed fiber laser. Traditional SAs, such as semiconductor saturable absorber mirrors (SESAM) and Fe^{2+}: ZnSe crystal, have been successfully employed to generate MIR pulsed fiber

lasers. Whereas, it has many inherent disadvantages reflected in the complicated and expensive manufacturing process, as well as the narrow operating band.

Since the discovery of the atomic-layer graphene, two dimensional (2D) materials are studied widely to realize light modulation, owing to the broadband absorption, fast relaxation time and easy-fabrication procedures. Recently, the graphene and graphene-like low-dimensional materials [3]–[16] have been applied as SAs to generate the Q-switched pulses in MIR region. However, the performance of the pulsed MIR fiber laser needs to be improved, especially the nonlinear optical modulation components. Inspired by the requirements to develop high-power, stable MIR fiber lasers, it is necessary to explore the novel nonlinear optical materials and modulators.

With the evolvement from single-component to binary component nonlinear optical materials [17]–[21], the 2D ternary materials have exhibited special rare optoelectronic properties with the addition of a third element. The bandgap can be tuned between the characteristic bandgaps of the two constituting binary compounds [22], [23]. As a ternary chalcogenide family member, the Ta_2NiS_5 portrays attractive physical properties which show obviously 2D characteristics and a huge in-plane anisotropy. This shows undeniable coupling among the 1-D chain structure via the angle-resolved high-resolution photoemission spectroscopy [24]. There are three sets of chain structures in Ta_2NiS_5, allowing considerable in-plane anisotropy of electrical and optical properties [25-27]. Moreover, the monolayer Ta_2NiS_5 has a 0.36 eV direct bandgap, and the bulk Ta_2NiS_5 exhibits a 0.39 eV direct bandgap [28], which shows that it has great potential in broadband applications. Recently, Ta_2NiS_5 SAs have been demonstrated to accomplish Q-switched and mode-locked fiber lasers at 1029 nm, 1569 nm [29] and 1.9 μm waveband [30]. However, the non-linear optical response and laser application based on the layered Ta_2NiS_5 have not been explored above 2 μm mid-infrared region, which can strongly prove the great potential of Ta_2NiS_5 as a broadband nonlinear material.

Here, the few-layer Ta_2NiS_5-SA was fabricated successfully using simple liquid phase exfoliation (LPE) method and deposited on the gold mirror. By Z-scan measurement, the nonlinear saturable absorption property of few-layer Ta_2NiS_5 was investigated. Based on the Ta_2NiS_5 SA, a stable passively Q-switched Er^{3+}-doped ZBLAN fiber laser at 2.8 μm has been demonstrated successfully experimentally.

The authors are with the Key Laboratory for Micro/Nano Optoelectronic Devices of Ministry of Education & Hunan Provincial Key Laboratory of Low-Dimensional Structural Physics and Devices, School of Physics and Electronics, Hunan University, Changsha 410082, China (e-mail: duanqw@hnu.edu.cn; yangll@hnu.edu.cn; 690927954@qq.com; llchen@hnu.edu.cn; jiezai@hnu.edu.cn; lilimiao@hnu.edu.cn; cjzhao@hnu.edu.cn).
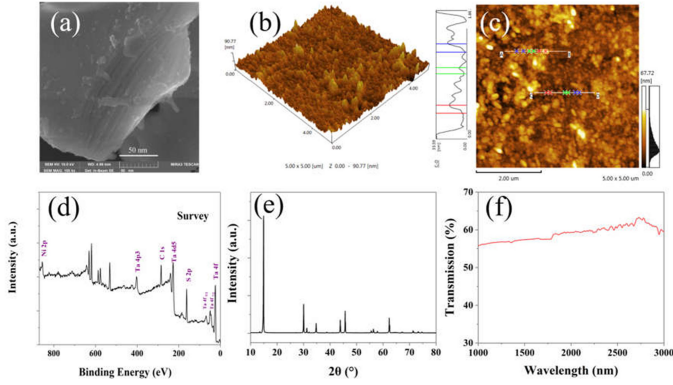
Fig. 1. (a) SEM image of the layered Ta_2NiS_5. (b) The surface morphology of Ta_2NiS_5 measured by AFM. (c) The surface thickness parameter of Ta_2NiS_5 measured by AFM. (d) The X-ray photoelectron spectroscopy (XPS) of the multilayered Ta_2NiS_5. (e) XRD pattern of Ta_2NiS_5 powder. (f) Linear transmission spectrum of the Ta_2NiS_5 placed on a CaF_2 substrate.

II. MATERIAL CHARACTERIZATIONS

The few-layered Ta_2NiS_5 was fabricated utilizing a simple liquid phase exfoliation (LPE) method with the Ta_2NiS_5 powder (Six Carbon Technology) [26], [28], which is a convenient and cost-effective way for fabricating low-dimensional materials. A high-purity Ta_2NiS_5 single crystal was grounded in an agar mortar, and then dissolved in N-Methyl pyrrolidone (NMP) and sonicated for more than 4 hours to ensure dispersion of large particles. The ice begs were then used to lower the temperature during ultrasonication to prevent overheating of the solution. At five-thousand rpm for a quarter an hour, the solution was then centrifuged and the Ta_2NiS_5 supernatant was deposited on the gold mirror, and then dried for 24 hours under an infrared oven lamp.

The structure of layered Ta_2NiS_5 was visualized by the electron-scanning microscopy (SEM) as shown in Fig. 1(a). A relatively smooth surface of the Ta_2NiS_5 film was observed through surface morphology under an atomic force microscope (AFM) measurement, as shown in Fig. 1(b). It can be found from Fig. 1(c) that layered Ta_2NiS_5 are uniformly dispersed on the substrate. The mean thickness of the layered Ta_2NiS_5 is 16.6 nm corresponding to a 26 layers thickness [31]. The X-ray photoelectron spectroscopy (XPS) in Fig. 1(d) shows the elemental binding energies of the obtained layered Ta_2NiS_5. The Ta 4f shows three obvious peaks, 23.2 eV, 25.2 eV, and 28.3 eV, among which the two main peaks of 23.2 eV and 25.2 eV correspond to the Ta $4f_{7/2}$ and Ta $4f_{5/2}$ of Ta^{4+} in Ta_2NiS_5, respectively [27], [32]. Ni 2p shows the main peaks 854.0 eV, which were fitted to the binding energies of Ni^{2+} in Ta_2NiS_5 [27], [33]. Two main peaks located at 161.5 and 162.7 eV were fitted as the dominant state of the S^{2-} in Ta_2NiS_5 [27]. The X-ray diffraction pattern (XRD) of the Ta_2NiS_5 powder shown in Fig. 1(e) meets its characteristics under normal conditions [27], which confirmed that the composition of the powder was Ta_2NiS_5. Fig. 1(f) displays that the layered Ta_2NiS_5 was placed on a CaF_2 substrate and its linear transmission spectrum was measured between 1000 nm and 3000 nm, which has a transmittance about 60%.
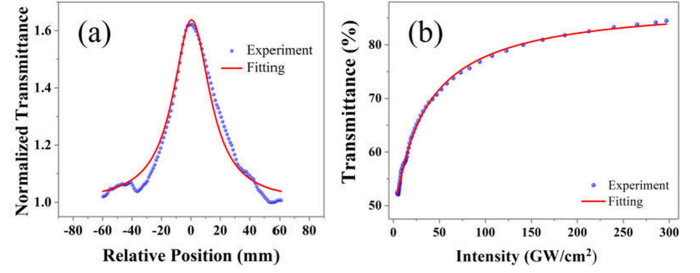

Fig. 2. The saturable absorption characteristics of Ta_2NiS_5 at 2800 nm. (a) Open-aperture Z-scan curves; (b) Nonlinear transmittance curve.

The narrow bandgap endows the layered Ta_2NiS_5 to exhibit broadband resonant absorption above 3 μm. With the increasing intensity of the incident light, the saturable absorption of the layered Ta_2NiS_5 can be realized via the Pauli-blocking principle. With the help of femtosecond laser setting at a repetition rate of 1 kHz and a pulse width of 35 fs working at 2800 nm wavelength, the nonlinear optical absorption behavior of the few-layered Ta_2NiS_5 was characterized with the open aperture Z-scan technique, as demonstrated in Fig. 2. The measurement results of Z-scan can be analyzed by the formula:

$$T(z) = 1 - \frac{q_0}{2\sqrt{2}\left(1 + z^2/z_0{}^2\right)} \qquad (1)$$

where Z_0 is the Rayleigh length, and $q_0 = \beta I_0 L_{eff}$, and β is the nonlinear absorption coefficient, and I_0 is the pulse intensity measured at the focus, and L_{eff} is the effective length of sample. The saturation intensity and modulation depth can be obtained by fitting the experimental data with the equation:

$$T(I) = 1 - \Delta T \exp(-I/I_s) - T_{ns} \qquad (2)$$

where $T(I)$ is the transmission, and ΔT is the modulation depth, and I, I_s and T_{ns} are incident pulse intensity, saturation intensity and non-saturation loss, respectively. The modulation depth of Ta_2NiS_5 is 36% and the saturation intensity of Ta_2NiS_5 is 32.2 GW/cm^2 according to the fitting result.

III. RESULTS AND DISCUSSIONS

The experiment setup of the Q-switched Er^{3+}-doped ZBLAN fiber laser based on Ta_2NiS_5-SAM is shown in Fig. 3, and the inset shows the real photo of the Ta_2NiS_5-SAM. A fiber-coupled 976 nm laser diode (105 μm core diameter and NA = 0.15) with 50 W maximum output power is collimated and focused by plano-convex lens L1 (Thorlabs N-BK7, f = 25.4 mm) and plano-convex lens L2 (Thorlabs CaF_2, f = 50 mm). Between the two lenses, a dichroic mirror M1 (High transmittance to pump light and high reflection to laser 2.8 μm) was set at 45° angle corresponding to the pump light and laser. A 3.9 m double-cladding Er^{3+}-doped (7 mol% doping concentration) ZBLAN fiber (Le Verre Fluoré, France) was used as the gain medium, which has a 15 μm diameter core and 0.12 numerical aperture. The ends of fiber were fixed in stainless-steel V-grooves then perpendicularly cleaved at the front end to provide Fresnel reflection and acted as the laser output coupler, meanwhile
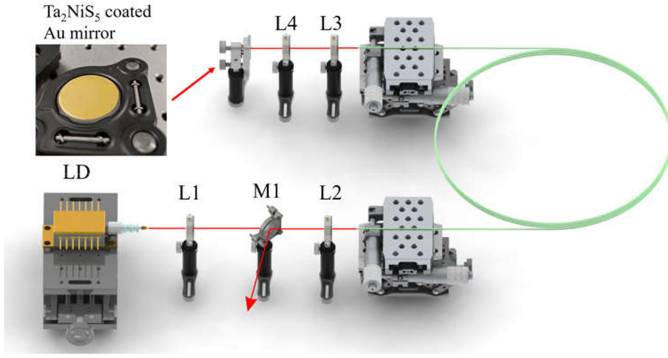
Fig. 3. Experiment schematic of Q-switched Er^{3+}:ZBLAN fiber laser based on ternary chalcogenide Ta$_2$NiS$_5$-SA. Inset, the real photo of the Ta$_2$NiS$_5$-SAM.

Fig. 5. (a) The relationship between repetition rate and pulse width with pump power. (b) The curve of output power and single pulse energy varying with the pump power.
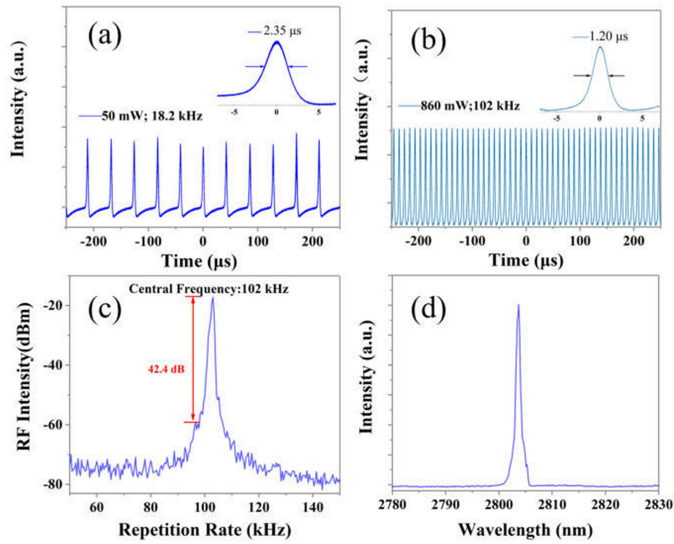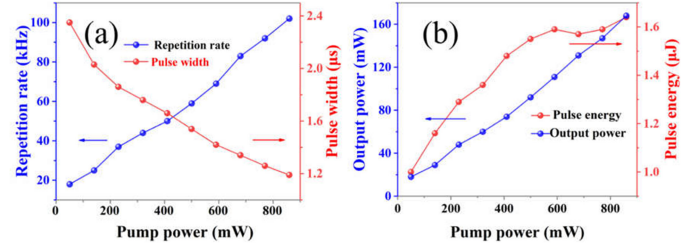

Fig. 4. (a) Q-switched pulse sequences delivered at pump power of 50 mW and (b) Q-switched pulse sequences delivered at a max pump power of 860 mW. The single pulse is shown in the inset. (c) RF spectrum characteristics and (d) optical spectrum characteristics.

the rear end was cleaved at an 8° angle to avoid the parasitic oscillation. Two 20 mm focal-length plano-convex CaF$_2$ lenses L3, L4 was used to make the 2.8 μm radiation accurately parallel and focused on the Ta$_2$NiS$_5$-SAM, which is served as SA and the terminated cavity feedback. The reflectivity of the Ta$_2$NiS$_5$ coated mirror at 2.8 μm is about 51.3%. Eventually, the resonator based on Ta$_2$NiS$_5$-SA was completed to realize the fiber laser oscillation. The optical spectrum was then measured by a 0.1 nm scanning resolution mid-infrared spectrometer. The frequency spectral was monitored by a highly sensitive spectral analyzer to furtherly obtain signal-to-noise ratio (SNR), and the pulse trains were monitored by 4 GHz bandwidth oscilloscope with the use of an HgCdTe detector.

The passively Q-switched pulse can be observed upon an increment of the pump power to 50 mW. Fig. 4(a) shows the pulse trains characteristics with 18.2 kHz repetition rate at this pump power, and the pulse width of 2.35 μs could be observed in the inset. Maintaining a stable Q-switching pulse trains is simple before exceeding the 860 mW pump power.

From Fig. 4(b) and inset, the repetition rate and pulse duration can be obtained about 1.20 μs and 102.4 kHz at 860 mW pump power, respectively. The non-optimized deposition procedure can't guarantee the film quality, which will lower the damage threshold of the SAM, and thus the available pump power and the output power. We measured the RF spectrum of the Q-switched pulse at the highest 860 mW pump power, as demonstrated in Fig 4(c). The SNR of the Ta$_2$NiS$_5$-SAM based Q-switched pulse trains were greater than 42 dB, which indicates its high stability and excellent characteristics of Ta$_2$NiS$_5$-SA. Fig. 4(d) shows the optical spectrum with 2803.7 nm central wavelength, along with the 3-dB bandwidth about 0.8 nm. The relationship between repetition rate and pulse width with pump power are shown in Fig. 5(a). The pulse width decreases as the pump power increases. Conversely, the repetition rate increases as the pump power increases. The repetition rate ranges from 18.2 kHz to 102.4 kHz, and the corresponding pulse width varies from 2.35 μs to 1.20 μs. Fig. 5(b) shows that both the output power and the single pulse energy change with the pump power. The output power increases almost linearly with the pump power with a slope of 18.5%, but the single pulse energy increases slowly as the pump increases. Eventually, the highest stable output power and single pulse energy obtained are 168 mW and 1.64 μJ, respectively.

Table I has summarized the typical recent reports of the $\sim$3 μm pulsed fiber lasers modulated by some 2D-materials. From the experimental results, the Ta$_2$NiS$_5$ shows stable nonlinear optical response and excellent Q-switched laser performance, especially the signal-to-noise ratio (SNR), which is important for the practical laser applications. In addition, the Ta$_2$NiS$_5$-SAM has shown stable physicochemical property and nearly the same optical response even after two months. We will optimize the Ta$_2$NiS$_5$-based saturable absorber and the cavity configuration to realize the mode-locking operation in our future work.

IV. CONCLUSION

In conclusion, we demonstrated the Q-switched ZBLAN fiber laser operation with the few-layered Ta$_2$NiS$_5$ prepared by LPE method. With the Ta$_2$NiS$_5$ SAM, the Q-switched ZBLAN fiber laser has delivered the stable pulses with the SNR of 42.4 dB, repetition rate 102 kHz, and pulse width 1.20 μs successfully at 2.8 μm wavelength. The experimental results validate the broadband nonlinear optical response of

TABLE I
TYPICAL PULSED MID-INFRARED FIBER LASER MODULATED BY 2D MATERIALS

SAs	λ_s (μm)	τ (ns)	SNR (dB)	Modulation Depth (%)	Saturation Intensity	Refs.
Graphene	2.78	0.042	43.5	10	2 MW/cm^2	[4]
Black phosphorus	2.97	2740	37.7	41.2	3.77 MW/cm^2	[7]
Bi_2Te_3	2.98	1370	37.4	51.3	2.12 MW/cm^2	[10]
$NiTe_2$	2.80	708	33	17.7	0.12 MW/cm^2	[13]
WS_2	2.87	1730	40.5	29.4	1.24 MW/cm^2	[14]
MoS_2	2.75	806	40	5	6.8 mJ/cm^2	[15]
$PtSe_2$	2.87	620	30	39.6	74 MW/cm^2	[16]
Ta_2NiS_5	2.80	1200	42.4	36	32.2 GW/cm^2	**This work**

the layered ternary chalcogenide in the mid-infrared region, and indicate that the ternary chalcogenides have great application potential in the high-performance MIR optoelectronic devices.

REFERENCES

[1] B. J. Eggleton, B. Luther-Davies, and K. Richardson, "Chalcogenide photonics," *Nature Photon.*, vol. 5, no. 3, pp. 141–148, 2011.

[2] A. B. Seddon, Z. Tang, D. Furniss, S. Sujecki, and T. M. Benson, "Progress in rare-earth-doped mid-infrared fiber lasers," *Opt. Exp.*, vol. 18, no. 25, pp. 26704–26719, 2010.

[3] C. Wei *et al.*, "Graphene Q-switched 2.78 μm er^{3+}-doped fluoride fiber laser," *Opt. Lett.*, vol. 38, no. 17, pp. 3233–3236, 2013.

[4] G. Zhu *et al.*, "Graphene mode-locked fiber laser at 2.8 μm," *IEEE Photon. Technol. Lett.*, vol. 28, no. 1, pp. 7–10, 2016.

[5] J. Liu, J. Xu, and P. Wang, "Graphene-based passively Q-switched 2 μm thulium-doped fiber laser," *Opt. Commun.*, vol. 285, no. 24, pp. 5319–5322, 2012.

[6] Z. Qin *et al.*, "Black phosphorus as saturable absorber for the Q-switched er: ZBLAN fiber laser at 2.8 μm," *Opt. Exp.*, vol. 23, no. 19, pp. 24713–24718, 2015.

[7] X. Liu and Y. Cui, "Revealing the behavior of soliton buildup in a mode-locked laser," *Adv. Photon.*, vol. 1, no. 1, 2019, Art. no. 016003.

[8] Z. Qin *et al.*, "Mode-locked 2.8-μm fluoride fiber laser: From soliton to breathing pulse," *Adv. Photon.*, vol. 1, no. 6, 2019, Art. no. 065001.

[9] P. Tang *et al.*, "2.8- μm pulsed Er^{3+}: ZBLAN fiber laser modulated by topological insulator," *IEEE Photon. Technol. Lett.*, vol. 28, no. 14, pp. 1573–1576, Jul. 2016.

[10] J. Li *et al.*, "3-μm mid-infrared pulse generation using topological insulator as the saturable absorber," *Opt. Lett.*, vol. 40, no. 15, pp. 3659–3662, 2015.

[11] C. Zhao *et al.*, "Ultra-short pulse generation by a topological insulator based saturable absorber," *Appl. Phys. Lett.*, vol. 101, no. 21, 2012, Art. no. 211106.

[12] W. Gao *et al.*, "Broadband photocarrier dynamics and nonlinear absorption of PLD-grown WTe$_2$ semimetal films," *Appl. Phys. Lett.*, vol. 112, no. 17, 2018, Art. no. 171112.

[13] L. Yang *et al.*, "Broadband optical response of layered nickel ditelluride towards the mid-infrared regime," *Opt. Mater. Exp.*, vol. 10, no. 5, pp. 1335–1343, 2020.

[14] C. Wei *et al.*, "Passively Q-switched mid-infrared fluoride fiber laser around 3 μm using a tungsten disulfide (WS$_2$) saturable absorber," *Laser Phys. Lett.*, vol. 13, no. 10, pp. 105108, 2016.

[15] S. Wang, Y. Tang, J. Yang, H. Zhong, and D. Fan, "MoS$_2$ Q-switched 2.8 μm er: ZBLAN fiber laser," *Laser Phys*, vol. 29, no. 2, pp. 025101, 2019.

[16] C. Wei, H. Chi, S. Jiang, L. Zheng, H. Zhang, and Y. Liu, "Long-term stable platinum diselenide for nanosecond pulse generation in a 3-μm mid-infrared fiber laser," *Opt. Exp.*, vol. 28, no. 22, pp. 33758–33766, 2020.

[17] W. Zhao *et al.*, "Origin of indirect optical transitions in few-layer MoS$_2$, WS$_2$, and WSe$_2$," *Nano Lett*, vol. 13, no. 11, pp. 5627–5634, 2013.

[18] Z. Ye *et al.*, "Probing excitonic dark states in single-layer tungsten disulphide," *Nature*, vol. 513, no. 7517, pp. 214–218, 2014.

[19] D. Mao *et al.*, "WS$_2$ saturable absorber for dissipative soliton mode locking at 1.06 and 1.55 μm," *Opt. Exp.*, vol. 23, no. 21, pp. 27509–27519, 2015.

[20] L. Du *et al.*, "Broadband nonlinear optical response of single-crystalline bismuth thin film," *ACS Appl. Mater. Inter.*, vol. 11, no. 39, pp. 35863–35870, 2019.

[21] L. Du *et al.*, "Antimony thin film as a robust broadband saturable absorber," *IEEE J. Sel. Topics Quantum Electron.*, vol. 27, no. 2, pp. 1–7, Mar./Apr. 2021.

[22] H. Ahmad *et al.*, "Ternary MoWSe$_2$ alloy saturable absorber for passively Q-switched Yb-, Er-and Tm-doped fiber laser," *Opt. Commun.*, vol. 437, pp. 355–362, 2019.

[23] T. Gao *et al.*, "2D Ternary chalcogenides," *Adv. Opt. Mater.*, vol. 6, no. 14, 2018, Art. no. 1800058.

[24] K. Mu *et al.*, "Electronic structures of layered Ta$_2$NiS$_5$ single crystals revealed by high-resolution angle-resolved photoemission spectroscopy," *J. Mater. Chem. C*, vol. 6, no. 15, pp. 3976–3981, 2018.

[25] A. Geldert *et al.*, "Single-layer ternary chalcogenide nanosheet as a fluorescence-based 'capture-release' biomolecular nanosensor," *Small*, vol. 13, no. 5, 2017, Art. no. 1601925.

[26] H. Zhu *et al.*, "Ternary chalcogenide nanosheets with ultrahigh photothermal conversion efficiency for photoacoustic theranostics," *Small*, vol. 13, no. 16, 2017, Art. no. 1604139.

[27] C. Tan *et al.*, "High-yield exfoliation of ultrathin two-dimensional ternary chalcogenide nanosheets for highly sensitive and selective fluorescence DNA sensors," *J. Amer. Chem. Soc.*, vol. 137, no. 32, pp. 10430–10436, 2015.

[28] L. Li *et al.*, "Strong in-plane anisotropies of optical and electrical response in layered dimetal chalcogenide," *ACS Nano*, vol. 11, no. 10, pp. 10264–10272, 2017.

[29] M. Ma *et al.*, "Ternary chalcogenide Ta$_2$NiS$_5$ nanosheets for broadband pulse generation in ultrafast fiber lasers," *Nanophotonics*, vol. 9, no. 8, pp. 2341–2349, 2020.

[30] B. Yan *et al.*, "Ternary chalcogenide Ta$_2$NiS$_5$ as a saturable absorber for a 1.9 μm passively Q-switched bulk laser," *Opt. Lett.*, vol. 44, no. 2, pp. 451–454, 2019.

[31] S. A. Sunshine and J. A. Ibers, "Structure and physical properties of the new layered ternary chalcogenides tantalum nickel sulfide (Ta$_2$NiS$_5$) and tantalum nickel selenide (Ta$_2$NiSe$_5$)," *lnorg. Chem.*, vol. 24, no. 22, pp. 3611–3614, 1985.

[32] H. Crawack and C. Pettenkofer, "Calculation and XPS measurements of the Ta4f CDW splitting in cu, cs and li intercalation phases of 1T-TaX$_2$ (X = s, se)," *Solid State Commun*, vol. 118, no. 7, pp. 325–332, 2001.

[33] D. L. Legrand, H. W. Nesbitt, and G. M. Bancroft, "X-ray photoelectron spectroscopic study of a pristine millerite (NiS) surface and the effect of air and water oxidation," *Amer. Mineral.*, vol. 83, no. 12, pp. 1256–1265, 1998.